

Supporting Information

Stability and decomposition pathways of the NiOOH OER active phase of NiOx electrocatalysts at open circuit potential traced by ex-situ and in-situ spectroscopies

Julia Gallenberger^{*a}, Harol Moreno Fernández^a, Mohan Li^{b,c}, Chuanmu Tian^a, Achim Alkemper^a, Bernhard Kaiser^a, and Jan Philipp Hofmann^{*a}

Characterization of the pristine sample

Before any electrochemical investigations, the nature of the thin films has been spectroscopically investigated. This is important as the initial state of the sample affects the time-stability of the NiOOH phase, as it is outlined in the article.

Figure S1 shows a Raman spectrum of a pristine NiO thin film of 120 nm thickness on a polished gold substrate. The spectrum is an overlap of three species: NiO from the bulk phase, Ni(OH)₂ as surface layer and carbon as a contamination. The vibrations of NiO are located in the lower wavenumber region and resemble literature spectra of nanocrystalline NiO.¹ Distinct phonon and magnon scattering appears at ~380 cm⁻¹ (1TO), ~420 cm⁻¹ (1TO), ~460 cm⁻¹ (1TO), ~520 cm⁻¹ (1P+1M), ~1100 cm⁻¹, and ~1500 cm⁻¹ (2M).^{1,2} The latter two are overlapping with the carbon D- and G-band at ~1330 cm⁻¹ and 1602 cm⁻¹ respectively.³ Above 3000 cm⁻¹, α-Ni(OH)₂ is detected with O-H stretching modes from intercalated water at 3240 cm⁻¹, 3410 cm⁻¹ and 3620 cm⁻¹. The exclusion of β-Ni(OH)₂ can be done due to the missing characteristic sharp vibration at ~3580 cm⁻¹. A lower vibrational mode for the present α-Ni(OH)₂, which is dominant in literature, appears at ~460 cm⁻¹.⁴⁻⁶ To validate its contribution we measured a sample of 6 nm NiO which was fully transformed by 800 CVs to Ni(OH)₂ and confirmed by XPS. For this sample, no peak was detected below 1000 cm⁻¹ due to the low Raman scattering cross section of this phase or high structural disorder (see Figure S3).^{7,8} We can conclude that the surface layer of Ni(OH)₂ in Figure S1 is not detected at low wavenumbers.

The presence of α-Ni(OH)₂, but not β-Ni(OH)₂ is also drawn from the FTIR reflectance spectra. Again, β-Ni(OH)₂ would show a sharp O-H stretching mode, in IR at ~3640 cm⁻¹. The maximum at ~510 cm⁻¹ is attributed to NiO as it is the only prominent band appearing for samples deposited shortly before in vacuum, where only a very thin surface Ni(OH)₂ layer was formed.⁹⁻¹¹ Vibrations at ~1420 cm⁻¹, ~1560 cm⁻¹, ~1650 cm⁻¹, ~3450 cm⁻¹, and 3580 cm⁻¹ point to ions and hydrogen bonded hydroxyl groups intercalated in α-Ni(OH)₂.^{5,12} In the range of 2900 cm⁻¹ vibrations of hydrocarbons are appearing.¹³ Our observations conform with literature reports that α-Ni(OH)₂ is the surface phase formed by hydroxylation of NiO in air, water or alkaline solution.^{8,14}

X-ray photoelectron spectroscopy reveals the dimension of the surface hydroxyl layer. As XPS is a surface sensitive technique and NiO vibrations are still clearly visible, the hydroxyl layer formed in air can only be a few nm thick.

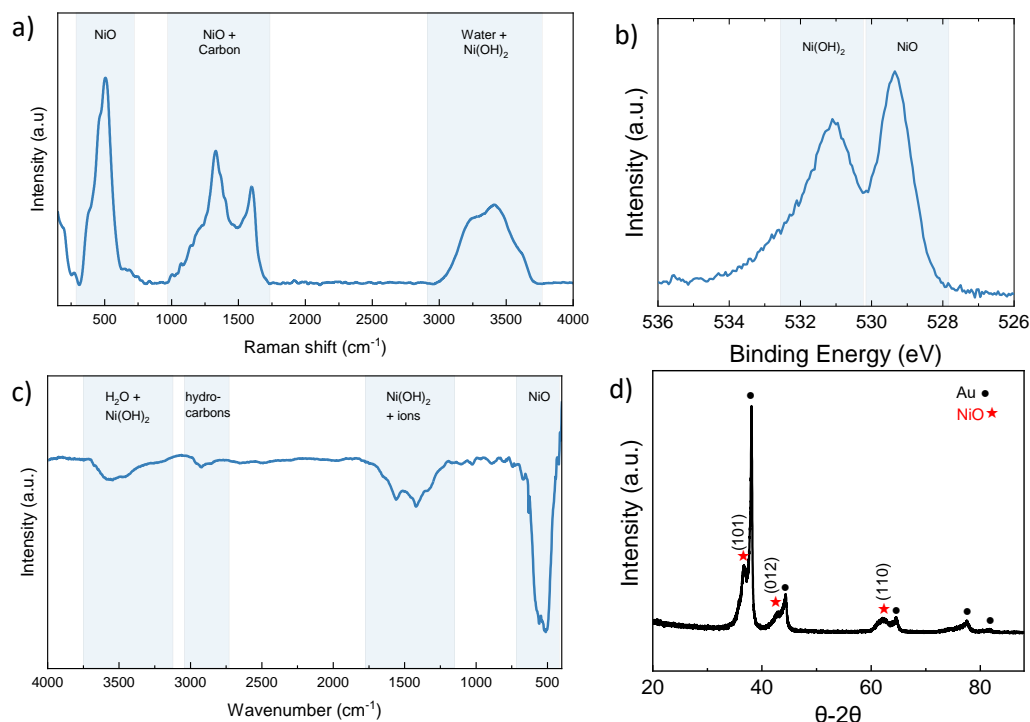


Figure S1: a) Raman (633 nm laser), b) XPS spectrum, c) FTIR, and d) GIWAXS of a pristine 120 nm NiO thin film. Peaks of the NiO and surface Ni-hydroxyl layer are detected.

Conditioning of the NiO thin films

The conditioning of the NiO thin films to transform more NiO to Ni(OH)₂ was done by performing 800 CVs over the Ni²⁺/Ni³⁺ redoxwaves (1.10-1.55 V vs. RHE, 100 mV/s), without going into the OER regime. Figure S2 shows the recorded CVs for the 120 nm and 6 nm thick NiO thin film.

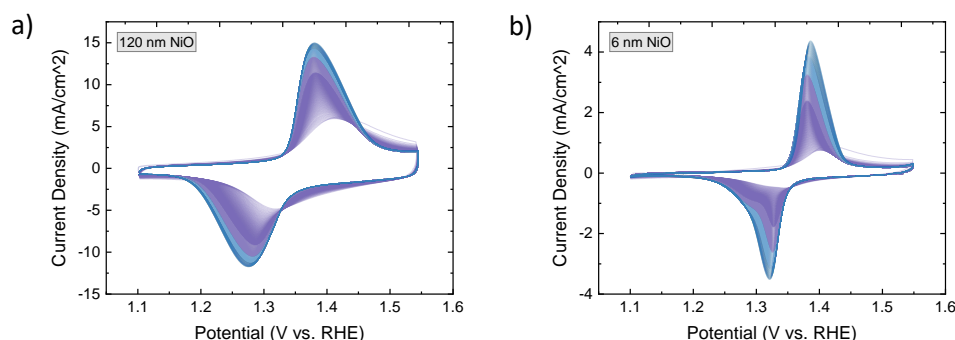


Figure S2: cyclic voltammograms of the conditioning of the a) 120 nm and b) 6 nm thick NiO samples investigated in our article. Both were activated with 800 CVs.

Assignment of features in Raman spectra

In the description of the Raman spectra in the article, we exclude Ni(OH)₂ vibrations, which is explained in the following.

Figure S3 a) shows the Raman spectra of a 6 nm thin film, that was transformed from NiO to almost exclusively Ni(OH)₂ by 800 CVs (compare XPS spectra of that sample, Figure 4 in the article). In the wavenumber region below 1200 cm⁻¹ no clear vibrations are detected. Therefore, the appearance of Ni(OH)₂ vibrations can be excluded in the 120 nm sample without conditioning, as the surface hydroxyl layer is much smaller in comparison (see XPS O1s in Figure S1).

The Raman spectra at a polarization of 1.50 V vs. RHE show the two E_{1g} and A_{1g} vibrations of NiOOH. Simultaneously there is a peak emerging at 600 cm⁻¹. This feature could be a Au-O vibration, which is blue-shifted by the deposition of the NiO overlayer.^{15,16} The presence of Au-oxide is reasonable, as the SEM images show cracks in the NiO film after electrochemistry, exposing the Au substrate to the electrolyte. In Figure S3 b) a cyclic voltammogram of a 120 nm thick sample is shown, that was treated with 200 CVs between 1.10-1.60 V vs. RHE and polarized at 1.90 V vs. RHE for 30 min. The result proves that the electrochemical treatment makes the Au substrate accessible to the electrolyte and prone to oxidation. As reference, Figure S3 c) shows the CVs of clean Au substrates after chronoamperometry at increasing potentials. However, a peak at about 600 cm⁻¹ also appears for samples measured on different substrates than Au. Therefore, we do not want to exclude that this feature could also be related to the NiOOH phase instead of a Au-O vibration.^{17,18}

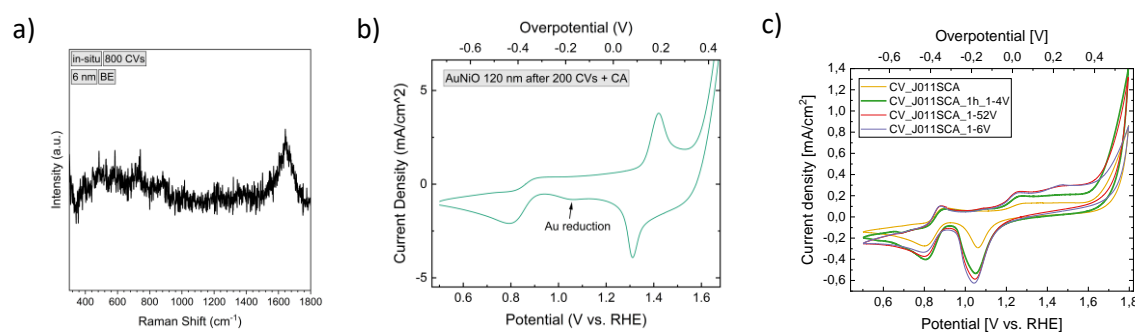


Figure S3: a) Raman spectrum of a 6 nm NiO film, activated by 800 CVs. No Ni(OH)₂ vibrations are detected at low wavenumbers. b) cyclic voltammogram of a 120 nm NiO film, activated by 200 CVs and polarized at 1.9 V vs. RHE beforehand. c) clean Au measured after chronoamperometry at increasing potentials.

Additional XPS spectra and fitting parameters of the O1s core level spectrum

The XPS spectra were all fitted using a Shirley background and a GL(30) line shape for the peaks. The sample of 6 nm in Figure 4 in the article shows mainly a Ni(OH)₂ peak at 531.3 eV and some remaining NiO at 529.1 eV.^{19,20} A peak at 532.9 eV was included for the carbon components on the surface.²¹ Its area is calculated from the respective C1s peak by using the R.S.F. value of 2.93 for the O1s core level. After chronoamperometry, two equally sized peaks were added for the oxy- and hydroxyl-group of NiOOH. To avoid overfitting, the following constraints on the remaining peaks were made: NiO and Ni(OH)₂ are kept at the same binding

energy like for the fit after 800 CVs, without NiOOH. The area of NiO was kept at about 4% of all Ni-related components in the O1s, because it was assumed to not be affected by CA. The area constraint is surely imprecise as the electron effective attenuation length (EAL) changes for a different layer system on top of NiO, but it was assumed to be more accurate than leaving out the NiO peak.

The area of the Ni2p line was also used to calculate the corresponding areas in the O1s line. Like this, the stoichiometry of approximately 2 oxygens per 1 Nickel atom could be confirmed.

The same constraints are applied for the fitting of the XPS spectra in Figure 6 in the article.

Additional spectra of the 6 nm NiO sample (Figure 4 in the article)

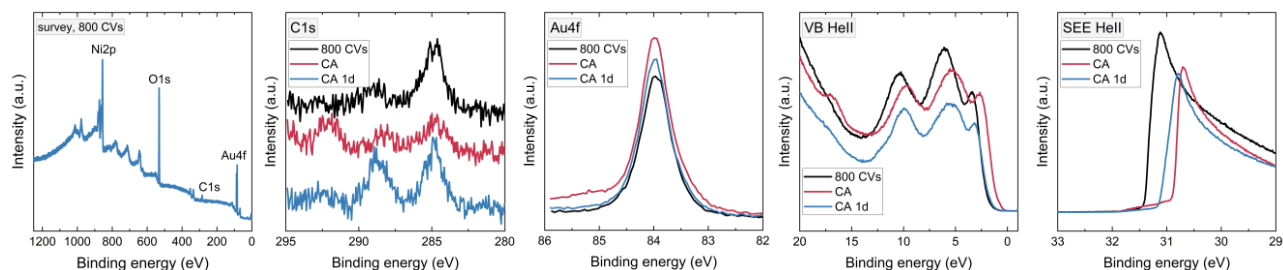


Figure S4: XPS survey, C1s, Au4f and UPS VB (valence band) and SEE (secondary electron cut-off) spectra of the 6 nm NiO sample.

Additional spectra of the 120 nm NiO sample (Figure 6 in the article)

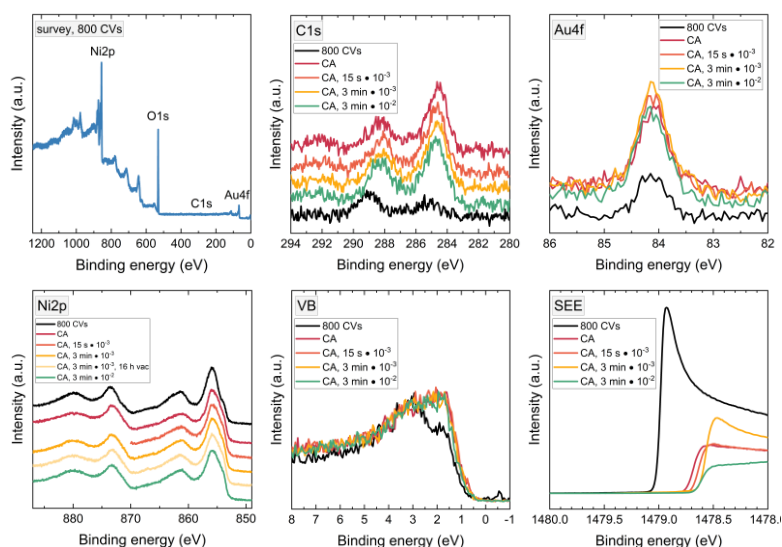


Figure S5: XPS survey, C1s, Au4f_{7/2}, Ni2p, VB, and SEE spectra of the 120 nm NiO sample.

Additional XPS data of the 120 nm sample – not rinsed

In the article, we show in Figure 5 Raman spectra of a 120 nm sample that was not rinsed after it was taken out immediately after polarization at 1.90 V vs. RHE. We show here in Figure S6 the corresponding XPS spectra. The C1s spectrum of the non-rinsed sample also includes 2 strong peaks at higher binding energy (292 eV and 295 eV), which correspond to the K2p doublet. The high potassium coverage is also evident by the strong K3p line, which was measured in the valence band by UPS at 16.6 eV. The peak at 288.6 eV in the C1s spectrum can be assigned to air-formed K₂CO₃.²² This surface layer is dampening the detection of the Ni2p electrons. In the O1s line, the contribution of OH-groups and formed potassium carbonate is combined to avoid overfitting. To compare the behaviour with the rinsed 120 nm sample, water adsorption was also performed on this sample. No change in the O1s means the H₂O did not affect the sample, which in turn means the NiOOH is not affected. This explains the stabilization of the NiOOH phase if the sample is not rinsed after the chronoamperometry. Storing the sample 1 d in air however, reduces the potassium coverage as the K₂CO₃ is hygroscopic and thereby draining off.²³ This is in line with our findings in Figure 4 in the article, where the NiOOH is finally reduced, even though it is first protected by the KOH / K₂CO₃ layer.

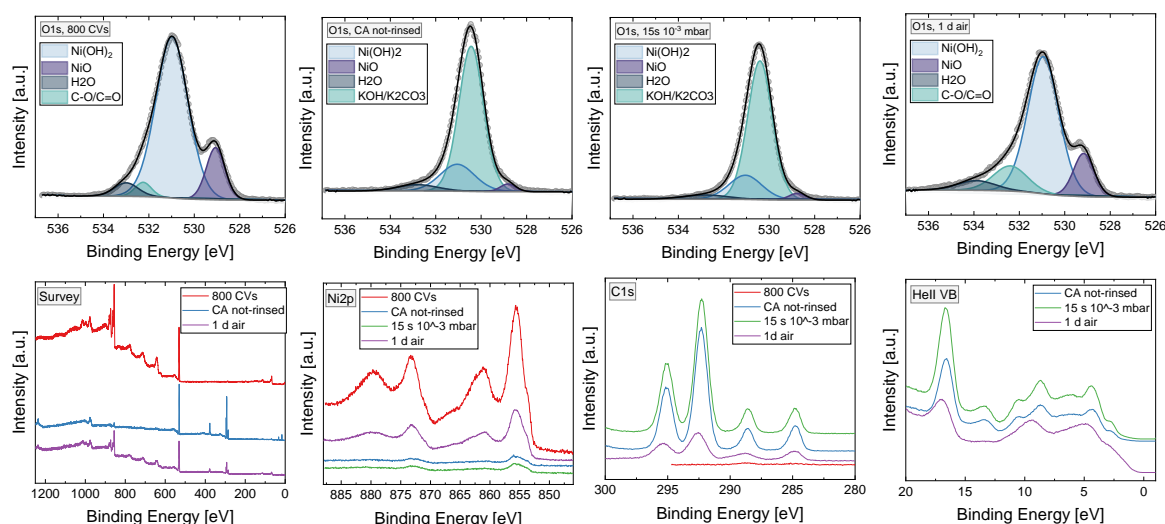


Figure S6: XPS O1s, survey, Ni2p, C1s and UPS VB spectra of the 120 nm NiO sample, that was not rinsed after electrochemistry. The evolution is shown starting from the activation with 800 CVs, chronoamperometry at 1.55 V vs. RHE without rinsing afterwards, exposure to $15 \text{ s} \cdot 10^{-3} \text{ bar H}_2\text{O}$ and storing it 1 d in air.

Experimental Details

Fourier Transform Infrared Spectroscopy

FTIR spectroscopy was done with a VERTEX 80v FTIR spectrometer (Bruker) from 4000 to 400 cm^{-1} . To this end, a room temperature DLaTGS detector was employed. Samples were measured on a monolayer / grazing angle specular reflectance accessory (Specac) at an incidence angle of 70° . For a background scan the polished gold surface was used. Both sample and background scans (250 scans each) were acquired with a scanner velocity of 2.5 kHz and a resolution of 4 cm^{-1} .

Inductively coupled plasma - optical emission spectrometry (ICP-OES)

ICP-OES was measured with the device iCAPTM PRO ICP-OES from Thermo ScientificTM, equipped with the Qtegra ISDS Software.

References

- 1 N. Mironova-Ulmane, A. Kuzmin, I. Sildos, L. Puust and J. Grabis, *Latv. J. Phys. Tech. Sci.*, 2019, **56**, 61–72.
- 2 N. Bala, H. K. Singh, S. Verma and S. Rath, *Phys. Rev. B*, 2020, **102**, 024423.
- 3 C. E. Taylor, S. D. Garvey and J. E. Pemberton, *Anal. Chem.*, 1996, **68**, 2401–2408.
- 4 S. Tao, Q. Wen, W. Jaegermann and B. Kaiser, *ACS Catal.*, 2022, **12**, 1508–1519.
- 5 D. S. Hall, D. J. Lockwood, S. Poirier, C. Bock and B. R. MacDougall, *J. Phys. Chem. A*, 2012, **116**, 6771–6784.
- 6 D. S. Hall, D. J. Lockwood, S. Poirier, C. Bock and B. R. MacDougall, *ACS Appl. Mater. Interfaces*, 2014, **6**, 3141–3149.
- 7 R. Kostecki and F. McLarnon, *J. Electrochem. Soc.*, 1997, **144**, 485.
- 8 D. S. Hall, C. Bock and B. R. MacDougall, *J. Electrochem. Soc.*, 2013, **160**, F235.
- 9 B. Subramanian, M. Mohamed Ibrahim, V. Senthilkumar, K. R. Murali, V. S. Vidhya, C. Sanjeeviraja and M. Jaya chandran, *Phys. B: Condens. Matter*, 2008, **403**, 4104–4110.
- 10 R. Cerc Korošec, P. Bukovec, B. Pihlar, A. Šurca Vuk, B. Orel and G. Dražič, *Solid State Ion.*, 2003, **165**, 191–200.
- 11 J. Li, W. Zhao, F. Huang, A. Manivannan and N. Wu, *Nanoscale*, 2011, **3**, 5103–5109.
- 12 R. Acharya, T. Subbaiah, S. Anand and R. P. Das, *Mater. Lett.*, 2003, **57**, 3089–3095.
- 13 A. E. Segneanu, I. Gozescu, A. Dabici, P. Sfirloaga, Z. Szabadai, A. E. Segneanu, I. Gozescu, A. Dabici, P. Sfirloaga and Z. Szabadai, *Organic Compounds FT-IR Spectroscopy. Macro To Nano Spectroscopy.*, IntechOpen, London, 2012.
- 14 D. Cappus, C. Xu, D. Ehrlich, B. Dillmann, C. A. Ventrice, K. Al Shamery, H. Kuhlenbeck and H.-J. Freund, *Chem. Phys.*, 1993, **177**, 533–546.
- 15 H.-C. Chen, C.-H. Chen, C.-S. Hsu, T.-L. Chen, M.-Y. Liao, C.-C. Wang, C.-F. Tsai and H. M. Chen, *ACS Omega*, 2018, **3**, 16576–16584.
- 16 B. S. Ye, S. L. Klaus, P. N. Ross, R. A. Mathies and A. T. Bell, *ChemPhysChem*, 2010, **11**, 1854–1857.
- 17 L. Bai, S. Lee and X. Hu, *Angewandte Chemie*, 2021, **133**, 3132–3140.
- 18 Y. L. Lo and B. J. Hwang, *Langmuir*, 1998, **14**, 944–950.
- 19 B. V. Crist, *Handbooks of Monochromatic XPS Spectra: Volume 2 : Commercially Pure Binary Oxides*, XPS International LLC, 2004.
- 20 M. C. Biesinger, B. P. Payne, A. P. Grosvenor, L. W. M. Lau, A. R. Gerson and R. St. C. Smart, *Appl. Surf. Sci.*, 2011, **257**, 2717–2730.
- 21 G. Beamson and D. Briggs, *High Resolution XPS of Organic Polymers - The Scienta ESCA300 Database*, Wiley Interscience, 1992.
- 22 K. Harting, U. Kunz and T. Turek, *Z. Phys. Chem.*, 2012, **226**, 151–166.
- 23 W. M. Haynes, Ed., *CRC Handbook of Chemistry and Physics*, CRC Press, Boca Raton, 95th edn., 2014.